IEEE Access
Multidisciplinary | Rapid Review | Open Access Journal

Received 13 July 2022, accepted 27 July 2022, date of publication 29 July 2022, date of current version 4 August 2022.

Digital Object Identifier 10.1109/ACCESS.2022.3195025

RESEARCH ARTICLE

Modeling and Detection of Phase Current Sensor Gain Faults in PMSM Drives

CIRO ATTAIANESE[1], (Senior Member, IEEE), MATILDE D'ARPINO[2], (Member, IEEE), MAURO DI MONACO[3], (Member, IEEE), AND LUIGI PIO DI NOIA[1], (Senior Member, IEEE)

[1]Department of Electrical Engineering and Information Technology, University of Naples "Federico II," 80125 Naples, Italy
[2]Center for Automotive Research, The Ohio State University, Columbus, OH 43212, USA
[3]Department of Electrical and Information Engineering, University of Cassino and Southern Lazio, 03043 Cassino, Italy

Corresponding author: Ciro Attaianese (ciro.attaianese@unina.it)

ABSTRACT The fault of current sensors in AC electric drives can cause inaccurate tracking of the control reference and torque oscillations, that can lead to damage of mechanical components. Therefore, the development of accurate detection techniques of these faults plays a crucial role for the proper management of the electric drive and for the fault isolation and estimation. In the paper, a model-based method for the detection of phase current sensor gain faults in a Permanent Magnet Synchronous Motor (PMSM) drive with Field Oriented Control (FOC) is proposed. At first, a mathematical model is presented, which allows an accurate determination of the analytical closed-form expression of the steady-state stator currents, taking into account the effects both of the current control regulators and of any current sensors gain faults. Starting from this model, a low-computation algorithm has been carried out, which allows not only to detect and isolate the current sensors affected by the gain fault, but also to estimate the gain values starting from the measured phase currents and motor speed. The model and the diagnostic algorithm performance is verified by means of numerical and experimental results.

INDEX TERMS Current sensor fault, PMSM drives, fault diagnosis.

I. INTRODUCTION

The high-power density and efficiency requirements of electric drives for electrified vehicles have led to a rapid spread of permanent magnet synchronous motors (PMSM) [1]–[4]. The performance of a PMSM drive strongly depends on the accurate measurement of electrical and mechanical quantities, such as motor phase currents, speed, and rotor position. However, these measurements can be affected by faults and deterioration of sensors performance, which can introduce offset and gain errors in the measured values [5], [6]. This is often due to the internal aging of the components of the sensor which are accelerated by external factors as humidity, extreme enviromental conditions, or are caused by electromagnetic interferences or mechanical vibrations. In recent years, issues related to the risk of cyber-attack have been investigated as well, as sensors are a vulnerable part of electric vehicles which can be manipulated to induce system failures [7]. Installation of redundant sensors can help to mitigate issues related to sensors' faults; however this is not feasible for many applications due to cost and/or volume limitations. Therefore, the development of diagnostic algorithms for the detection and isolation of sensor faults are required to guarantee the proper performance of an electric drive [8]. Various approaches for sensor faults' diagnosis have been proposed in literature; they can be classified into data-driven and model-based methods [9], [10]. Data-driven algorithms are not strictly dependent on the type of drive, but require to be trained with a large amount of data covering both normal and abnormal operating points of the drive [10]–[12]. These data are not always available and could be affected by noise and disturbances. Therefore, the performance of data-driven algorithms is heavily depending on the variety and quality of the data used to train the diagnostic algorithm. In several instances the data used for the algorithm calibration are derived from virtual experiments due to lack

The associate editor coordinating the review of this manuscript and approving it for publication was Guillermo Valencia-Palomo.

This work is licensed under a Creative Commons Attribution 4.0 License. For more information, see https://creativecommons.org/licenses/by/4.0/

of experimental results [13]. Model-based approaches are very well accepted diagnostic techniques which are based on the knowledge of the electric drive behavior and related modeling description [14], [15]. Model-based algorithms are often augmented with estimators or observers to cope with model uncertainties, parameter variations and response of the control loops.

In the context of sensor failures, special attention must be paid to the ones involving current sensors, due to their importance for the control and the monitoring of electric drives. A faulty phase current sensor can deviate from the true value because of an offset and/or a gain fault, as well as complete loss of the signal is possible [16].

This paper focuses on the study of the effects of the gain faults of the phase current sensors in a surface-mounted PMSM (SMPMSM) drive. These faults introduce variations in the measured motor currents with respect to the healthy sensor case, determining errors in the calculation of control reference commands, which give rise to torque and speed oscillations. Many solutions have been proposed in literature for the diagnosis of gain faults in phase current sensors. In [17], a comparison between three different machine learning algorithms based on linear regression, decision tree and neural network is performed for the diagnosis of phase current gain faults. Three features are extracted from virtual experiments data, such as peak to peak difference and variance of the phase current measurement. Other literature describe techniques able to compensate this type of fault in the control. A complex vector analysis of the phase current sensor gain-deviation errors is described in [18]. The proposed model is used to heuristically estimate the gain error and to develop a compensation algorithm. In [19] a method based on the Discrete Fourier Transform is proposed. By extracting the second harmonic component of the q-axis voltage command, the diagnostic algorithm is able to detect the phase current sensor gain fault. In [20] the compensation of gain error is carried out through the estimation of the voltage error from the control equations of the PMSM.

Many papers are devoted to the fault tolerant aspect as well. The aim of fault tolerance is to prevent faults from leading to system failure. To achieve this, techniques for identification, isolation and estimation of faults are combined with those for dealing with and compensating their effects [16], [21].

Unlike the approaches proposed so far in literature, this paper first develops the solution of the mathematical model of a SMPMSM drive with field oriented control (FOC), including also the effects of current control regulators, which is able to express in analytical closed form the steady-state motor currents when current gain sensor faults occur. Starting from this solution, a low-computation intensity algorithm is carried out, which allows not only to detect and isolate the current sensors affected by gain fault, but also to estimate the gain values of each sensor, starting from the measured phase currents and motor speed. Numerical and experimental results confirm that the proposed algorithm gives a good estimation of the gain values which can be directly used to provide a fault indicator index.

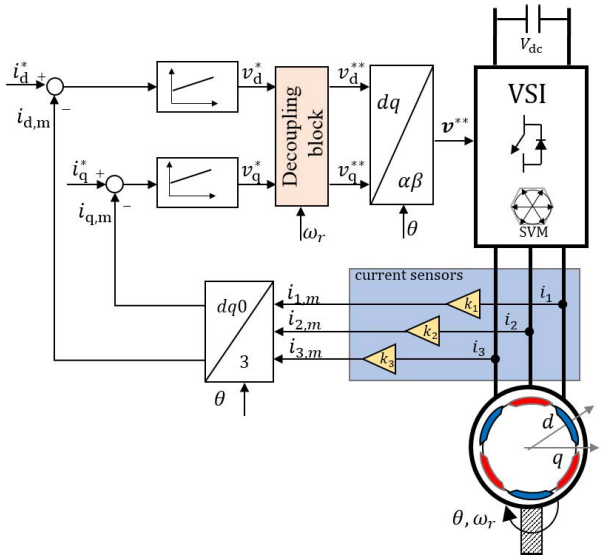

FIGURE 1. Schematic of the considered SMPMSM drive with field oriented control and SVM.

The organization of the paper is as follows: Section II describes the proposed modeling approach of the SMPMSM drive with FOC, when one or more current sensors gain faults are considered. The Section II is devoted to the numerical validation of the proposed model. The model-based algorithm for current sensor gain faults detection, isolation and estimation (FDIE) is described in Section IV, while Section V includes the numerical and experimental validation of the proposed FDIE algorithm. The conclusions are reported in the Section VI. Eventually, in the Appendix the detailed formulas on which the proposed algorithm is based are given.

II. MODELING OF SMPMSM DRIVE WITH GAIN FAULTS OF CURRENT SENSORS

A. MATHEMATICAL MODEL DEFINITION

Reference is made to a SMPMSM fed by a Voltage Source Inverter (VSI) and controlled by means of FOC strategy with Space Vector Modulation (SVM) (Fig.1). Making the well-known simplifyng assumptions, the mathematical model of a SMPMSM drive can be expressed by the following set of equations [22], [23]:

$$\begin{cases} v_{\mathrm{d}} = L\dfrac{\mathrm{d}i_{\mathrm{d}}}{\mathrm{d}t} + Ri_{\mathrm{d}} - p\omega_{\mathrm{r}}Li_{\mathrm{q}} \\ v_{\mathrm{q}} = L\dfrac{\mathrm{d}i_{\mathrm{q}}}{\mathrm{d}t} + Ri_{\mathrm{q}} + p\omega_{\mathrm{r}}Li_{\mathrm{d}} + p\omega_{\mathrm{r}}\phi \end{cases} \tag{1}$$

where v_{d}, v_{q}, i_{d}, i_{q} denote the d- and q-components of motor voltage and current space vectors in the rotor flux reference frame, R and L are the stator resistance and inductance, ω_{r} is the motor speed, p the pole pairs number, ϕ the rotor flux, and t the time.

The d- and q-axes voltage references, v_d^* and v_q^*, are generated by two PI controllers, having as input the errors between

the reference current components i_{d}^{*}, i_{q}^{*}, and the measured ones $i_{\mathrm{d,m}}$, $i_{\mathrm{q,m}}$. To take into account of the cross-coupling terms in (1) a decoupling block is required, which is defined by the following equations:

$$\begin{cases} v_{\mathrm{d}}^{**} = v_{\mathrm{d}}^{*} - p\omega_{\mathrm{r}} L i_{\mathrm{q,m}} \\ v_{\mathrm{q}}^{**} = v_{\mathrm{q}}^{*} + p\omega_{\mathrm{r}} L i_{\mathrm{d,m}} + p\omega_{\mathrm{r}}\phi \end{cases} \tag{2}$$

Thus, the reference space vector $\boldsymbol{v}^{**}$of the supply voltage in the stator reference frame is given by:

$$\boldsymbol{v}^{**} = (v_{\mathrm{d}}^{**} + \mathrm{j}v_{\mathrm{d}}^{**})\,\mathrm{e}^{\mathrm{j}p\theta} \tag{3}$$

where θ is the rotor mechanical angle, and j represents the unit imaginary number. Including the feedback control action of the PI controllers, the model of the drive becomes:

$$\begin{cases} k_{\mathrm{Pd}}(i_{\mathrm{d}}^{*} - i_{\mathrm{d,m}}) + k_{\mathrm{Id}} \displaystyle\int_0^t (i_{\mathrm{d}}^{*} - i_{\mathrm{d,m}})\,\mathrm{d}t - p\omega_{\mathrm{r}} L i_{\mathrm{q,m}} \\ \qquad = L\dfrac{\mathrm{d}i_{\mathrm{d}}}{\mathrm{d}t} + Ri_{\mathrm{d}} - p\omega_{\mathrm{r}} L i_{\mathrm{q}} \\ k_{\mathrm{Pq}}(i_{\mathrm{q}}^{*} - i_{\mathrm{q,m}}) + k_{\mathrm{Iq}} \displaystyle\int_0^t (i_{\mathrm{q}}^{*} - i_{\mathrm{q,m}})\,\mathrm{d}t + p\omega_{\mathrm{r}} L i_{\mathrm{d,m}} \\ \qquad = L\dfrac{\mathrm{d}i_{\mathrm{q}}}{\mathrm{d}t} + Ri_{\mathrm{q}} + p\omega_{\mathrm{r}} L i_{\mathrm{d}} \end{cases} \tag{4}$$

where k_{Pd}, k_{Pq}, k_{Id}, k_{Iq} are the gains of the PI controllers. If all the phase current sensors are healthy it is:

$$i_{\mathrm{d,m}} = i_{\mathrm{d}} \quad i_{\mathrm{q,m}} = i_{\mathrm{q}} \tag{5}$$

and the solution of (4) allows to determine the current components i_{d} and i_{q} provided that the motor speed is known and constant. When a fault occurs in the sensor of the h-th phase current, the measured current $i_{h,\mathrm{m}}$, and the actual current i_{h} will be different, and therefore it will be also:

$$i_{\mathrm{d,m}} \neq i_{\mathrm{d}} \quad i_{\mathrm{q,m}} \neq i_{\mathrm{q}} \tag{6}$$

To solve (4) when a sensor current fault occurs, the d- and q-components $i_{\mathrm{d,m}}$ and $i_{\mathrm{q,m}}$ of the measured currents have to be determined as a function of i_{d} and i_{d}. To get this result, if the phase current sensors are affected by gain fault, the measured currents can be expressed as:

$$i_{h,\mathrm{m}} = k_{\mathrm{h}} i_{\mathrm{h}} \quad \text{with} \quad h = 1, 2, 3 \tag{7}$$

where the coefficient k_h represents the gain of the h-th current sensor. Obviously, if k_h is equal to one, the sensor is healthy. In α and β stator coordinates, denoting with $\boldsymbol{i}$ and $\boldsymbol{i}_{\mathrm{m}}$ the space vectors of the actual and of the measured motor current, respectively, it is:

$$\boldsymbol{i} = \frac{2}{3}\sum_{h=1}^{3} i_h\,\mathrm{e}^{\frac{2\pi}{3}(h-1)} = i_\alpha + \mathrm{j}i_\beta \tag{8}$$

$$\boldsymbol{i}_{\mathrm{m}} = \frac{2}{3}\sum_{h=1}^{3} i_{h,\mathrm{m}}\,\mathrm{e}^{\frac{2\pi}{3}(h-1)} = i_{\alpha,\mathrm{m}} + \mathrm{j}i_{\beta,\mathrm{m}} \tag{9}$$

while in terms of d- and q-axes components it is:

$$\boldsymbol{i} = (i_{\mathrm{d}} + \mathrm{j}i_{\mathrm{q}})\,\mathrm{e}^{\mathrm{j}p\theta} \quad \boldsymbol{i}_{\mathrm{m}} = (i_{\mathrm{d,m}} + \mathrm{j}i_{\mathrm{q,m}})\,\mathrm{e}^{\mathrm{j}p\theta} \tag{10}$$

Combining (7), (8), (9), (10) gives:

$$\begin{bmatrix} i_{\mathrm{d,m}} \\ i_{\mathrm{q,m}} \end{bmatrix} = \begin{bmatrix} s + w_1 & w_2 \\ w_2 & s - w_1 \end{bmatrix} \begin{bmatrix} i_{\mathrm{d}} \\ i_{\mathrm{q}} \end{bmatrix} \tag{11}$$

with:

$$\begin{cases} w_1 = q\cos(2p\theta) + r\sin(2p\theta) \\ w_2 = r\cos(2p\theta) - q\sin(2p\theta) \end{cases} \tag{12}$$

and

$$\begin{cases} q = \dfrac{1}{3}k_1 - \dfrac{1}{6}(k_2 + k_3) \\ r = \dfrac{\sqrt{3}}{6}(-k_2 + k_3) \\ s = \dfrac{1}{3}(k_1 + k_2 + k_3) \end{cases} \tag{13}$$

Equation (11) allows to express $i_{\mathrm{d,m}}$ and $i_{\mathrm{q,m}}$ as a function of i_{d} and i_{q}. If constant speed is assumed, that is:

$$\theta(t) = \omega_{\mathrm{r}} t \tag{14}$$

substituting (11) in (4) and taking the derivative gives:

$$\begin{cases} L\dfrac{\mathrm{d}i_{\mathrm{d}}^2}{\mathrm{d}t^2} + z_1\dfrac{\mathrm{d}i_{\mathrm{d}}}{\mathrm{d}t} + z_2\dfrac{\mathrm{d}i_{\mathrm{q}}}{\mathrm{d}t} + z_3 i_{\mathrm{d}} + z_4 i_{\mathrm{q}} = k_{\mathrm{id}} i_{\mathrm{d}}^{*} \\ L\dfrac{\mathrm{d}i_{\mathrm{q}}^2}{\mathrm{d}t^2} + y_1\dfrac{\mathrm{d}i_{\mathrm{d}}}{\mathrm{d}t} + y_2\dfrac{\mathrm{d}i_{\mathrm{q}}}{\mathrm{d}t} + y_3 i_{\mathrm{d}} + y_4 i_{\mathrm{q}} = k_{\mathrm{iq}} i_{\mathrm{q}}^{*} \end{cases} \tag{15}$$

where

$$\begin{cases} z_1 = R + (w_1 + s)k_{\mathrm{pd}} + w_2 p\omega_{\mathrm{r}} L \\ z_2 = w_2 k_{\mathrm{pd}} - (w_1 - s + 1)p\omega_{\mathrm{r}} L \\ z_3 = 2w_2 p\omega_{\mathrm{r}} k_{\mathrm{pd}} - 2\,w_1 p^2\omega_{\mathrm{r}}^2 L + (w_1 + s)k_{\mathrm{id}} \\ z_4 = -2w_1 p\omega_{\mathrm{r}} k_{\mathrm{pd}} - w_2(2p^2\omega_{\mathrm{r}}^2 L - k_{\mathrm{id}}) \\ y_1 = w_2 k_{\mathrm{pq}} - (w_1 + s - 1)p\omega_{\mathrm{r}} L \\ y_2 = R - (w_1 - s)k_{\mathrm{pq}} - w_2 p\omega_{\mathrm{r}} L \\ y_3 = -2w_1 p\omega_{\mathrm{r}} k_{\mathrm{pq}} - w_2(2p^2\omega_{\mathrm{r}}^2 L - k_{\mathrm{iq}}) \\ y_4 = -2w_2 p\omega_{\mathrm{r}} k_{\mathrm{pq}} + 2w_1 p^2\omega_{\mathrm{r}}^2 L - (w_1 - s)k_{\mathrm{iq}} \end{cases} \tag{16}$$

B. STEADY-STATE ANALYTICAL SOLUTION

Assuming that the inverter modulation is ideal, the solution of (15) allows to analytically determine the current components i_{d} and i_{q} for any value of the gains k_1, k_2 and k_3 of the current sensors, taking into account the gains of the PI controllers. It should be noted that, despite the presence of the decoupling block in the control loop, the two equations of the system (15) are no longer decoupled when a gain fault of one or more phase current sensors occurs. For determining the steady-state solution of the system (15) in analytical closed form, the method of undetermined coefficients can be used [24], [25]. Thus, a steady-state solution has the form:

$$\begin{cases} i_{\mathrm{d}}(t) = \displaystyle\sum_{h=1}^{n}\left[a_{\mathrm{d},h}\cos(2hp\omega_r t) + b_{\mathrm{d},h}\sin(2hp\omega_r t)\right] + c_{\mathrm{d}} \\ i_{\mathrm{q}}(t) = \displaystyle\sum_{h=1}^{n}\left[a_{\mathrm{q},h}\cos(2hp\omega_r t) + b_{\mathrm{q},h}\sin(2hp\omega_r t)\right] + c_{\mathrm{q}} \end{cases} \tag{17}$$

with

$$\begin{cases} \lim\limits_{h\to\infty} a_{\mathrm{d},h} = 0 & \lim\limits_{h\to\infty} b_{\mathrm{d},h} = 0 \\ \lim\limits_{h\to\infty} a_{\mathrm{q},h} = 0 & \lim\limits_{h\to\infty} b_{\mathrm{q},h} = 0 \end{cases} \tag{18}$$

In other words, when a gain fault of one or more current sensors occurs, the d-q current components are given by the sum of a series of harmonics having $2hp\omega_\mathrm{r}$ angular frequency, with h integer. The coefficients $a_{\mathrm{d},h}$, $b_{\mathrm{d},h}$, $a_{\mathrm{q},h}$, $b_{\mathrm{q},h}$, c_d, c_q are functions of motor parameters, motor speed, controller gains, and current sensor gains, and they must be determined in such a way that the currents $i_\mathrm{d}(t)$ and $i_\mathrm{q}(t)$ given by (17) are solutions of system (15). Imposing this condition yields:

$$\begin{cases} \sum\limits_{k=1}^{n+1}\left[f_{\mathrm{d},k}\cos(2pk\omega_\mathrm{r}t) + g_{\mathrm{d},k}\sin(2pk\omega_\mathrm{r}t)\right] + f_{d,0} = k_\mathrm{id}i_\mathrm{d}^* \\ \sum\limits_{k=1}^{n+1}\left[f_{\mathrm{q},k}\cos(2pk\omega_\mathrm{r}t) + g_{\mathrm{q},k}\sin(2pk\omega_\mathrm{r}t)\right] + f_{q,0} = k_\mathrm{iq}i_\mathrm{q}^* \end{cases} \tag{19}$$

where $f_{\mathrm{d},0}$, $f_{\mathrm{q},0}$, $f_{\mathrm{d},k}$, $g_{\mathrm{d},k}$, $f_{\mathrm{q},k}$, $g_{\mathrm{q},k}$ are linear functions of the coefficients $a_{\mathrm{d},h}$, $b_{\mathrm{d},h}$, $a_{\mathrm{q},h}$, $b_{\mathrm{q},h}$, c_d, c_q, which have to be determined by solving the following system:

$$\begin{cases} f_{\mathrm{d},0}\left(a_{\mathrm{d},h}, b_{\mathrm{d},h}, a_{\mathrm{q},h}, b_{\mathrm{q},h}, c_\mathrm{d}, c_\mathrm{q}\right) = k_\mathrm{id}i_\mathrm{d}^* \\ f_{\mathrm{q},0}\left(a_{\mathrm{d},h}, b_{\mathrm{d},h}, a_{\mathrm{q},h}, b_{\mathrm{q},h}, c_\mathrm{d}, c_\mathrm{q}\right) = k_\mathrm{iq}i_\mathrm{q}^* \\ f_{\mathrm{d},k}\left(a_{\mathrm{d},h}, b_{\mathrm{d},h}, a_{\mathrm{q},h}, b_{\mathrm{q},h}, c_\mathrm{d}, c_\mathrm{q}\right) = 0 \\ g_{\mathrm{d},k}\left(a_{\mathrm{d},h}, b_{\mathrm{d},h}, a_{\mathrm{q},h}, b_{\mathrm{q},h}, c_\mathrm{d}, c_\mathrm{q}\right) = 0 \\ f_{\mathrm{q},k}\left(a_{\mathrm{d},h}, b_{\mathrm{d},h}, a_{\mathrm{q},h}, b_{\mathrm{q},h}, c_\mathrm{d}, c_\mathrm{q}\right) = 0 \\ g_{\mathrm{q},k}\left(a_{\mathrm{d},h}, b_{\mathrm{d},h}, a_{\mathrm{q},h}, b_{\mathrm{q},h}, c_\mathrm{d}, c_\mathrm{q}\right) = 0 \end{cases} \tag{20}$$

with $h \in \{1, \ldots, n\}$ and $k \in \{1, \ldots, (n+1)\}$. The analytical expressions of the functions $f_{\mathrm{d},0}, f_{\mathrm{q},0}, f_{\mathrm{d},k}, g_{\mathrm{d},k}, f_{\mathrm{q},k}, g_{\mathrm{q},k}$ are given in the appendix.

Equations (20) represent an overdetermined system of linear equations, having $(4n+6)$ equations and $(4n+2)$ unknowns. It can be expressed in matrix form:

$$A\boldsymbol{x} = \boldsymbol{b} \tag{21}$$

where the system matrix A is a $(4n+6)\times(4n+2)$ matrix, and where:

$$\boldsymbol{x}^\mathrm{T} = \left[c_\mathrm{d} \quad c_\mathrm{q} \quad \underbrace{a_{\mathrm{d},h} \quad b_{\mathrm{d},h} \quad a_{\mathrm{q},h} \quad b_{\mathrm{q},h}}_{h=1,\ldots,n}\right] \tag{22}$$

$$\boldsymbol{b}^\mathrm{T} = \left[k_\mathrm{id}i_\mathrm{d}^* \quad k_\mathrm{iq}i_\mathrm{q}^* \quad \underbrace{0 \quad 0 \quad \ldots \quad 0 \quad 0}_{4(n+1)\text{ zero elements}}\right] \tag{23}$$

To solve the system of linear equations (21), a new system matrix A' has to be considered, which must be a square submatrix of the matrix A, having order $(4n+2)\times(4n+2)$, chosen in such a way that its rank is $(4n+2)$ and that the resulting system of equations has a solution other than the trivial one. It is immediate to verify that the last four equations of system (20), obtained for $k = n+1$, always contain only the unknowns $a_{\mathrm{d},n}$, $b_{\mathrm{d},n}$, $a_{\mathrm{q},n}$, $b_{\mathrm{q},n}$, that is:

$$\begin{cases} f_{\mathrm{d},n+1}\left(a_{\mathrm{d},n}, b_{\mathrm{d},n}, a_{\mathrm{q},n}, b_{\mathrm{q},n}\right) = 0 \\ g_{\mathrm{d},n+1}\left(a_{\mathrm{d},n}, b_{\mathrm{d},n}, a_{\mathrm{q},n}, b_{\mathrm{q},n}\right) = 0 \\ f_{\mathrm{q},n+1}\left(a_{\mathrm{d},n}, b_{\mathrm{d},n}, a_{\mathrm{q},n}, b_{\mathrm{q},n}\right) = 0 \\ g_{\mathrm{q},n+1}\left(a_{\mathrm{d},n}, b_{\mathrm{d},n}, a_{\mathrm{q},n}, b_{\mathrm{q},n}\right) = 0 \end{cases} \tag{24}$$

and are linearly dependent, because the rank of the matrix of the homogeneous system (24) is always less than four, which implies that the number of solutions of system (24) is infinite. Moreover, due to (18) these equations are the least significant ones of system (20). Therefore, as matrix A' the one obtained eliminating the last four equations from system (20) can be assumed. Thus, it yields:

$$\boldsymbol{x} = \left(A'\right)^{-1}\boldsymbol{b} \tag{25}$$

As regards the choice of n, that is the number of terms to be considered for the analytical determination of the currents i_d and i_q expressed by (17), it should be noted that if the two PI controllers are the same, that is if:

$$k_\mathrm{pd} = k_\mathrm{pq} \quad k_\mathrm{id} = k_\mathrm{iq} \tag{26}$$

the exact solution of equations (15) is obtained for $n = 1$, that is the d-q current components contain only the harmonic having $2p\omega_\mathrm{r}$ angular frequency.

In the most general case, that is when (26) is not satisfied, the solution of (21) is the better approximated the greater is the value of n in (17). Obviously, the degree of approximation of the solution found for a given value of n depends on the values of the functions $f_{\mathrm{d},n+1}$, $g_{\mathrm{d},n+1}$, $f_{\mathrm{q},n+1}$, $g_{\mathrm{q},n+1}$ in correspondence of the solution found. In fact, if:

$$\bar{c}_\mathrm{d}, \bar{c}_\mathrm{q}, \bar{a}_{\mathrm{d},h}, \bar{b}_{\mathrm{d},h}, \bar{a}_{\mathrm{q},h}, \bar{b}_{\mathrm{q},h} \quad \text{with } h \in 1, \ldots, n \tag{27}$$

is the solution of (25), and $\bar{f}_{\mathrm{d},n+1}, \bar{g}_{\mathrm{d},n+1}, \bar{f}_{\mathrm{q},n+1}, \bar{g}_{\mathrm{q},n+1}$ are the corresponding values of the functions $f_{\mathrm{d},n+1}$, $g_{\mathrm{d},n+1}$, $f_{\mathrm{q},n+1}$, $g_{\mathrm{q},n+1}$, then the absolute values of the maximum errors in the determination of i_d and i_q, made assuming (27) as solution of (21), are given by:

$$\begin{cases} e_{\mathrm{d},n} = \sqrt{\bar{f}_{\mathrm{d},n+1}^2 + \bar{g}_{\mathrm{d},n+1}^2} & \text{for } i_\mathrm{d} \\ e_{\mathrm{q},n} = \sqrt{\bar{f}_{\mathrm{q},n+1}^2 + \bar{g}_{\mathrm{q},n+1}^2} & \text{for } i_\mathrm{q} \end{cases} \tag{28}$$

III. MODEL NUMERICAL VALIDATION

In order to validate the proposed model, a numerical analysis has been performed on the SMPMSM drive of tab. 1. The motor is fed by a VSI with SVM and controlled by means of FOC strategy according to the scheme of Fig.1. A simulation has been implemented in Matlab® Simulink and includes the d-q axes model of the SMPMSM, the FOC control loop, the two-level VSI, the phase currents measurement with the possibility to injecting the phase current gain faults. Both ideal modulation and SVM have been considered. In particular, a realistic model of the SVM inverter has been implemented, considering symmetric modulation, time delay due to the

acquisition, quantization error due to the 8-bit discretization of the modulation unit. All simulations have been carried out by using a maximum step size equal to 100 μs.

As regards the choice of n for the motor of tab.1, Fig.2, Fig.3 and Fig.4 show the maximum errors $e_{d,n}$, $e_{q,n}$ defined by (28) as a function of n for different values of the speed and of the current gains. In particular, the Fig.2 shows the errors in the case of zero gain of a single sensor, while the Fig.3 and Fig.4 are related to the case of reduction and increase of 50% of the gain of a single sensor, respectively. From the inspection of these figures it is immediate to note that the contribution of the terms obtained in (17) for $n > 3$ is very low. Therefore, $n = 3$ can be assumed with a very good approximation. In this case, if the solution is evaluated according to eq. (25), vectors $\mathbf{x}$ and $\mathbf{b}$ are given by:

$$\boldsymbol{x}^{\mathrm{T}} = \big[c_{\mathrm{d}} \quad c_{\mathrm{q}} \quad \underbrace{a_{\mathrm{d},h} \quad b_{\mathrm{d},h} \quad a_{\mathrm{q},h} \quad b_{\mathrm{q},h}}_{h=1,2,3}\big] \tag{29}$$

$$\boldsymbol{b}^{\mathrm{T}} = \big[k_{\mathrm{id}} i_{\mathrm{d}}^{*} \quad k_{\mathrm{iq}} i_{\mathrm{q}}^{*} \quad \underbrace{0 \quad 0 \quad \ldots \quad 0 \quad 0}_{12 \text{ zero elements}}\big] \tag{30}$$

while A' is a 14×14 matrix. The steady-state d- and q-current components will be given by:

$$\big[i_{\mathrm{d}} \quad i_{\mathrm{q}}\big] = \boldsymbol{x}^{\mathrm{T}} H = \big((A')^{-1}\boldsymbol{b}\big)^{\mathrm{T}} H \tag{31}$$

with:

$$H = \begin{bmatrix} 1 & 0 \\ 0 & 1 \\ \cos(2p\omega_{\mathrm{r}}t) & 0 \\ \sin(2p\omega_{\mathrm{r}}t) & 0 \\ 0 & \cos(2p\omega_{\mathrm{r}}t) \\ 0 & \sin(2p\omega_{\mathrm{r}}t) \\ \cos(4p\omega_{\mathrm{r}}t) & 0 \\ \sin(4p\omega_{\mathrm{r}}t) & 0 \\ 0 & \cos(4p\omega_{\mathrm{r}}t) \\ 0 & \sin(4p\omega_{\mathrm{r}}t) \\ \cos(6p\omega_{\mathrm{r}}t) & 0 \\ \sin(6p\omega_{\mathrm{r}}t) & 0 \\ 0 & \cos(6p\omega_{\mathrm{r}}t) \\ 0 & \sin(6p\omega_{\mathrm{r}}t) \end{bmatrix} \tag{32}$$

For the motor of tab.1, Figs.5, 6 and 7 show the comparison of the current components i_{d} and i_{q} obtained by simulation and by means of the proposed model for different values of the current gains in the case of ideal modulation. In particular, the Fig.5 is related to the case of a complete loss of one current sensor, while in Figs.6 and 7 are depicted the trends of the currents when the gains of one current sensor have a change of -50% and $+50\%$, respectively, with respect to the healthy case. As it is well highlighted by the reported trends, the proposed model accurately estimates the motor d-q current components, with a negligible error in the case of ideal modulation (RMS error less than 0.043%). Removing the hypothesis of ideal modulation, the results of i_{d} and i_{q} obtained for a SVM are reported in Figs.8, 9 and 10. The SVM has been numerically simulated considering a switching frequency of 20 kHz (tab.1). Also in this case, it is possible to note a good agreement between the model and the simulation results unless the unavoidable differences due to the ripple introduced by the SVM.

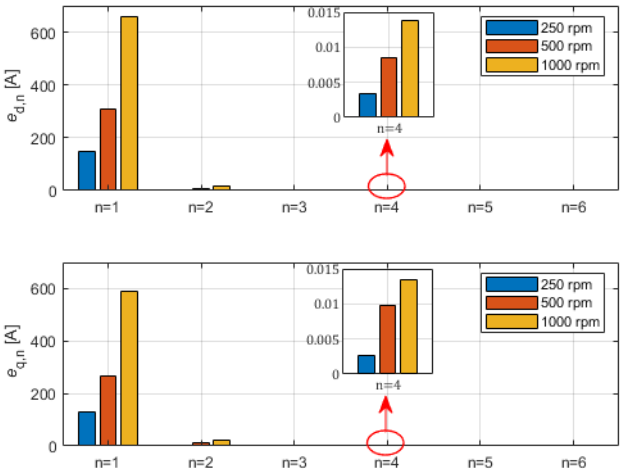

FIGURE 2. $e_{d,n}$ and $e_{q,n}$ in the case of zero gain of a single sensor, load torque 3.4 Nm.

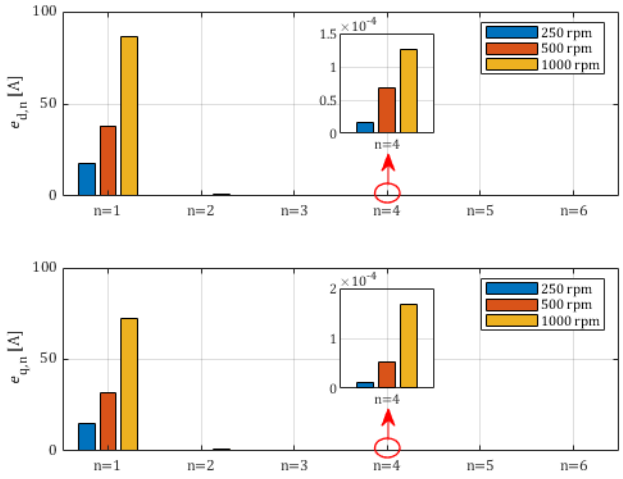

FIGURE 3. $e_{d,n}$ and $e_{q,n}$ in the case of a 50% gain reduction of a single sensor, load torque 3.4 Nm.

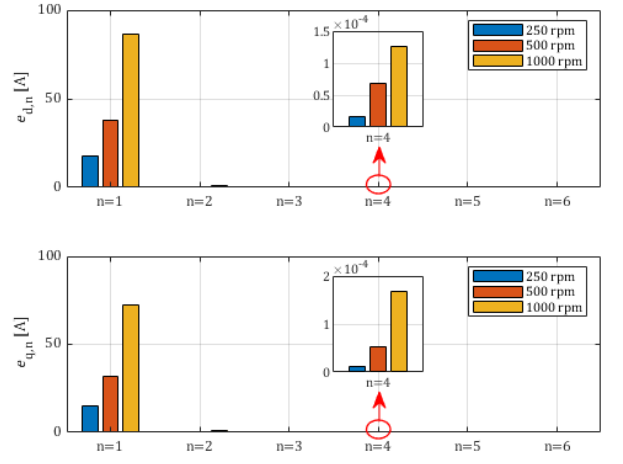

FIGURE 4. $e_{d,n}$ and $e_{q,n}$ in the case of a 50% gain increase of a single sensor, load torque 3.4 Nm.

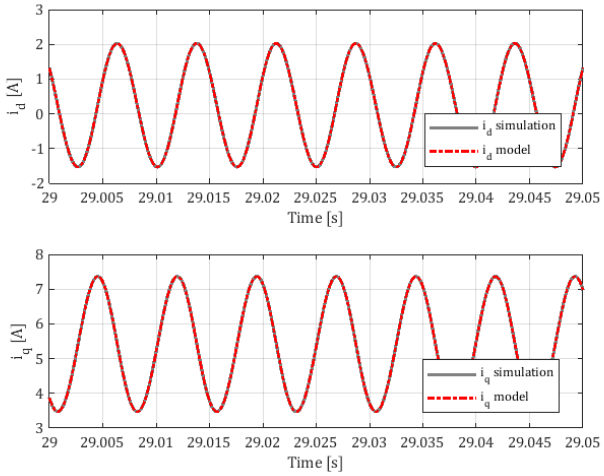

FIGURE 5. Current components i_d and i_q obtained by simulation (gray) and by the proposed model (red) in the case of $k_1 = 1$, $k_2 = 0$, $k_3 = 1$, ideal modulation, load torque 3.4 Nm, and angular speed 1000 rpm.

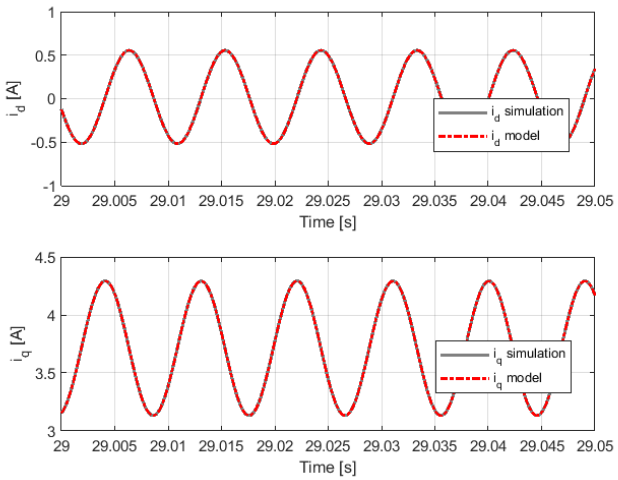

FIGURE 6. Current components i_d and i_q obtained by simulation (gray) and by the proposed model (red) in the case of $k_1 = 1$, $k_2 = 0.5$, $k_3 = 1$, ideal modulation, load torque 3.4 Nm, and angular speed 1000 rpm.

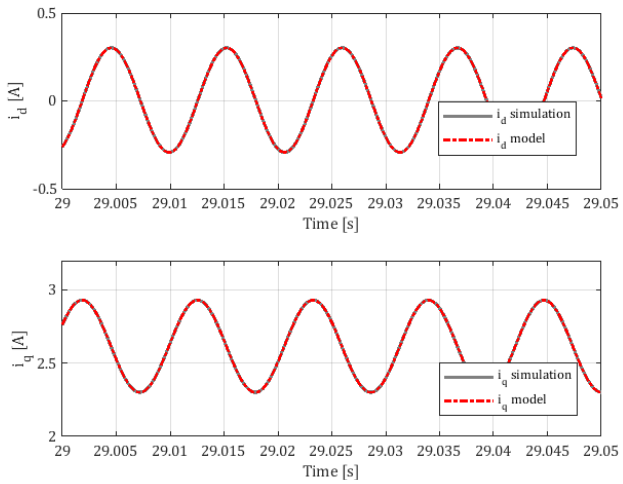

FIGURE 7. Current components i_d and i_q obtained by simulation (gray) and by the proposed model (red) in the case of $k_1 = 1$, $k_2 = 1.5$, $k_3 = 1$, ideal modulation, load torque 3.4 Nm, and angular speed 1000 rpm.

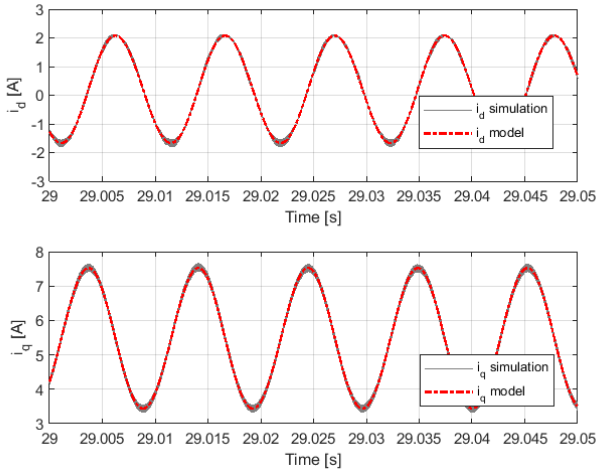

FIGURE 8. Current components i_d and i_q obtained by simulation (gray) and by the proposed model (red) in the case of $k_1 = 1$, $k_2 = 0$, $k_3 = 1$, SVM modulation, load torque 3.4 Nm, and angular speed 1000 rpm.

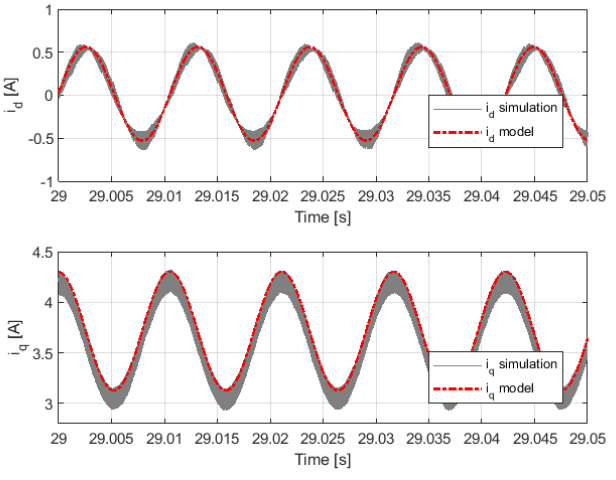

FIGURE 9. Current components i_d and i_q obtained by simulation (gray) and by the proposed model (red) in the case of $k_1 = 1$, $k_2 = 0.5$, $k_3 = 1$, SVM modulation, load torque 3.4 Nm, and angular speed 1000 rpm.

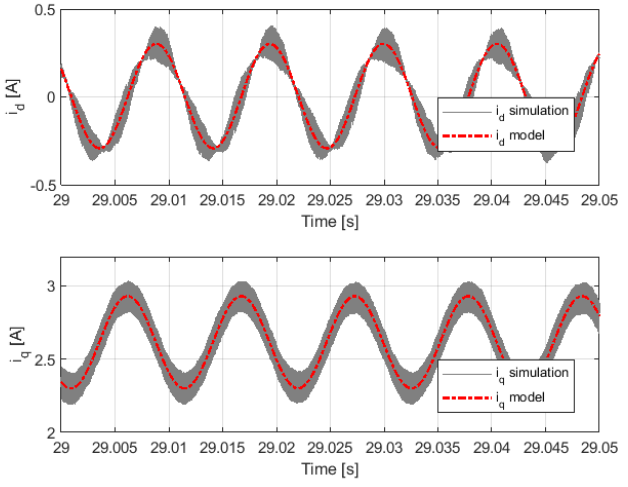

FIGURE 10. Current components i_d and i_q obtained by simulation (gray) and by the proposed model (red) in the case of $k_1 = 1$, $k_2 = 1.5$, $k_3 = 1$, SVM modulation, load torque 3.4 Nm, and angular speed 1000 rpm.

IV. DETECTION, ISOLATION AND ESTIMATION OF CURRENT SENSORS GAIN FAULT

The model developed in previous section can be used to set up an algorithm for detection, isolation and estimation (FDIE) of gain faults of the phase current sensors, based on the measurement and processing of the motor currents. In fact, combining (31) with (9) and (11) yields:

$$\begin{bmatrix} i_{\alpha,\mathrm{m}} \\ i_{\beta,\mathrm{m}} \end{bmatrix} = Q\left[G\left[\left((A')^{-1}\boldsymbol{b}\right)^{\mathrm{T}}H\right]^{\mathrm{T}}\right] \tag{33}$$

where, according to (9) and (11), it is:

$$G = \begin{bmatrix} s+w_1 & w_2 \\ w_2 & s-w_1 \end{bmatrix} \tag{34}$$

$$Q = \begin{bmatrix} \cos(p\omega_{\mathrm{r}}t) & -\sin(p\omega_{\mathrm{r}}t) \\ \sin(p\omega_{\mathrm{r}}t) & \cos(p\omega_{\mathrm{r}}t) \end{bmatrix} \tag{35}$$

Therefore, the motor measured currents will be:

$$\begin{cases} i_{1,\mathrm{m}} = i_{\alpha,\mathrm{m}} + i_{\mathrm{o,m}} \\ i_{2,\mathrm{m}} = -\dfrac{1}{2}i_{\alpha,\mathrm{m}} + \dfrac{\sqrt{3}}{2}i_{\beta,\mathrm{m}} + i_{\mathrm{o,m}} \\ i_{3,\mathrm{m}} = -\dfrac{1}{2}i_{\alpha,\mathrm{m}} - \dfrac{\sqrt{3}}{2}i_{\beta,\mathrm{m}} + i_{\mathrm{o,m}} \end{cases} \tag{36}$$

where $i_{\mathrm{o,m}}$ is the measured homopolar current, defined as:

$$i_{\mathrm{o,m}} = \frac{1}{3}\left(i_{1,\mathrm{m}} + i_{2,\mathrm{m}} + i_{3,\mathrm{m}}\right) \tag{37}$$

As a consequence of (33), (36) and (37), when a gain fault of one or more current sensors occurs, while the d-q current components are given by the sum of a series of harmonics having $2hp\omega_{\mathrm{r}}$ angular frequency, with h integer, the motor phase currents are instead expressed by the sum of a series of harmonics having $(2h-1)p\omega_{\mathrm{r}}$ angular frequency.

Starting from the measured currents $i_{1,\mathrm{m}}$, $i_{2,\mathrm{m}}$, $i_{3,\mathrm{m}}$, the set of equations (33), (36) and (37) can be regarded as a set of three equations in the unknowns q, r and s, which in turn allow to evaluate the gains k_1, k_2 and k_3 of the current sensors by means of (13). Therefore, from a strictly mathematical point of view, to determine the gains of the current sensors it is sufficient to acquire the measured phase currents $i_{1,\mathrm{m}}$, $i_{2,\mathrm{m}}$, $i_{3,\mathrm{m}}$ at a given time instant t^*, and solve the system formed by the set of equations (33), (36) and (37) in the unknowns q, r, s. Then, by means of (13), the values of k_1, k_2, and k_3 can be determined. However, in this way the estimate of k_1, k_2, and k_3 would inevitably be affected by the noise due to the modulation. To overcome this problem, the estimate of k_1, k_2, and k_3 was carried out by acquiring more samples of the measured phase currents in a given time interval, performing the FFT, and determining k_1, k_2, and k_3 in such a way to minimize the function:

$$\sum_{h=1}^{3}\left[I_{h,(p\omega_r),\mathrm{m}} - \hat{I}_{h,(p\omega_r)}\right]^2 \tag{38}$$

where $I_{h,(p\omega_r),\mathrm{m}}$ and $\hat{I}_{h,(p\omega_r)}$ are the amplitudes of the first harmonic of the current measured in the h-th phase, and the one calculated by means of the proposed model, respectively. Figure 11 shows the proposed FDIE algorithm scheme.

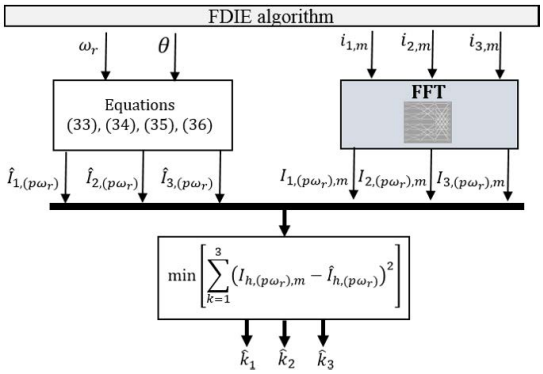

FIGURE 11. FDIE algorithm scheme for the sensor gains estimation The subscript $p\omega_r$ denotes the first harmonic of the measured and estimated currents.

From a theoretical point of view, since the proposed algorithm can calculate the value of each gain of the phase current sensors, it would also be able to compensate for sensor faults allowing the drive to continue operating, provided that the execution time of the algorithm is sufficiently small, in order to avoid damages due to the high torque oscillations. Because the fault tolerant control is not part of this work, the proposed algorithm has not been optimized as regards the execution time. It has been tested using a computing machine having an Intel CoreTM i7-10700 @ 2.90 GHz. It requires to acquire at least one period of the phase currents fundamental waveforms, while about 10 seconds are needed for the post processing.

V. EXPERIMENTAL VALIDATION OF THE PROPOSED FDIE ALGORITHM

The validation of the proposed FDIE algorithm has been performed by means of an experimental test bench. In particular, experimental tests have been carried out on a 1.23 kW three-phase SMPMSM manufactured by Control Techniques UNIMOTOR (Model: 95UMB300CACAA), whose parameters are given in Tab.1. A two-level three-phase VSI based on Mitsubishi PM100DSA120IPMs is adopted to drive the SMPMSM. The load is provided by a hysteresis dynamometer MAGTROL, Model HD-715-8NA. The inertia of the load is emulated through the coupling between the dynamometer and a flywheel. The motor is driven using a closed-loop torque control based on FOC strategy, according to the scheme of Fig.1. The control has been implemented using the DS1006 processor board of a dSPACE modular system, while the symmetrical modulation has been carried out by means of an Altera CPLD EPM7160SLC8410. The dSPACE processor is run with a 100μs synchronization signal: during this period, T_s, the control unit generates the inverter modulation pattern S_j (with j=1, . . . , 6) which will be imposed in the next T_s by the digital I/O board DS4003. The motor angular speed is measured using an incremental encoder, with 4096 ppr and a measurement quantization error of 1.92 rad/s. The output

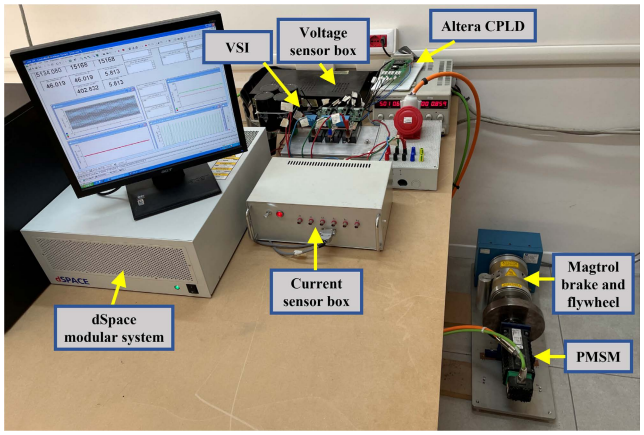

FIGURE 12. Experimental test bench adopted for the validation of the proposed model and FDIE algorithm.

TABLE 1. Parameters of the SMPMSM drive and of the control system.

SPMSM		
Rated power	1.23	kW
Rated torque $T_{\rm n}$	3.9	Nm
Rated speed $\omega_{\rm rn}$	314	rad/s
Rated current (rms)	2.7	A
Pole pairs	3	
Stator resistance R	3.7	Ω
Stator inductance L	0.012	H
Rotor flux ϕ	0.27	Wb
Motor inertia J	2.5e-4	kg · m^2
DC-link voltage $V_{\rm dc}$	600	V
Load		
Rated torque	6.5	Nm
Maximum speed	2,500	rpm
Maximum power	3.35	kW
Flywheel inertia (J)	0.06	kg · m^2
Control System		
$k_{\rm Pd}, k_{\rm Id}, k_{\rm Pq}, k_{\rm Iq}$	15, 9, 20, 10	
Processor frequency of DS1006 board	2.8	GHz
Max. frequency of DS3002 encoder board	750	kHz
Resolution of DS2004 A/D Board	16	bit
Switching frequency	10	kHz

of the encoder is transmitted to the DS3002 encoder board of dSPACE, while the DS2004 A/D board acquires the three phase currents measured by three LEM Current Transducers LA 25-NP, and the DC link voltage measured by a LEM Voltage Transducer CV3-1500. The experimental test bench is depicted in Fig.12 and the scheme of the control set-up is shown in Fig.13, including the proposed FDIE algorithm.

For the purposes of the following analyses, the gain faults of the phase current sensors are emulated by modifying the gains of the current sensors after the measurement chain in the DS1006 control code, as shown in Fig. 13. This allowed for easy estimating the performance of the proposed model and of the FDIE algorithm for different operating conditions. The main control system parameters are given in Table 1.

The comparison between the model and the experimental results obtained for different conditions of load and sensor gain values are reported in Figs.14, 15, 16 and 17. In particular, the figures show the comparison between the components

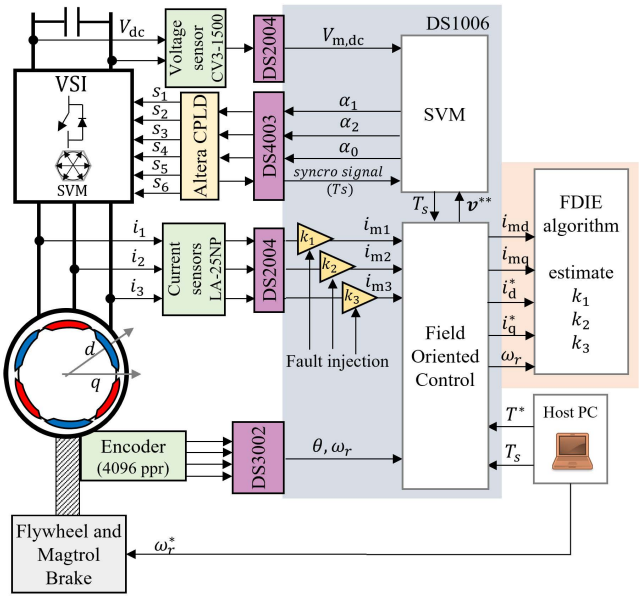

FIGURE 13. Structure of the control set-up including the FDIE algorithm implementation.

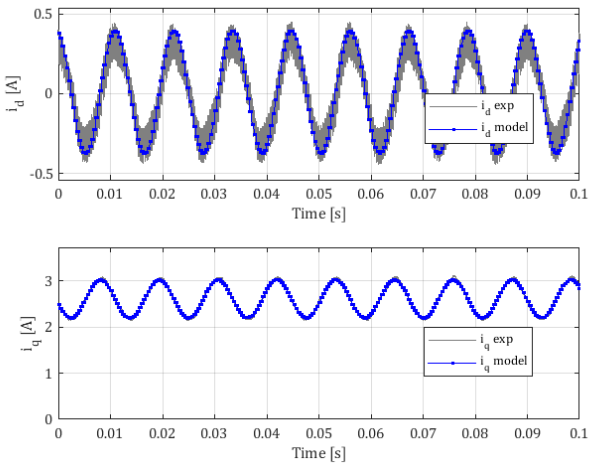

FIGURE 14. Current components $i_{\rm d}$ and $i_{\rm q}$ obtained by experimental test (gray) and by the proposed model (blue) in the case of $k_1 = 1$, $k_2 = 0.5$, $k_3 = 1$, load torque 2.3 Nm, and angular speed 1000 rpm.

$i_{\rm d}$ and $i_{\rm q}$ of motor currents calculated with the proposed model and measured ones by experimental tests when the motor speed is 1000 rpm and torque od 2.3 Nm and 3.4 Nm are considered. As already obtained from the comparison with the simulation results, also the experimental results highlight the good performance of the proposed analytical model.

Using the same condition of load, angular speed and sensor gain values, the developed FDIE algorithm has been tested. The good agreement between the FDIE algorithm and experimental results are confirmed by the comparison between the measured phase currents obtained for different gain faults, and the phase currents estimated by the proposed model considering the values of the current sensors gains calculated by the algorithm. In particular, the trends of the measured and estimated phase currents are depicted in

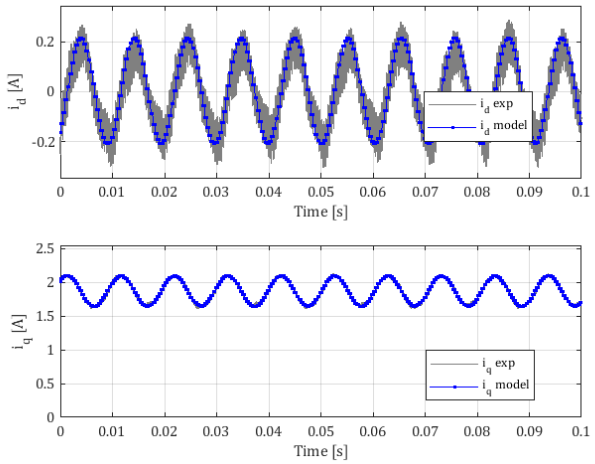

FIGURE 15. Current components i_d and i_q obtained by experimental test (gray) and by the proposed model (blue) in the case of $k_1 = 1$, $k_2 = 1.5$, $k_3 = 1$, load torque 2.3 Nm, and angular speed 1000 rpm.

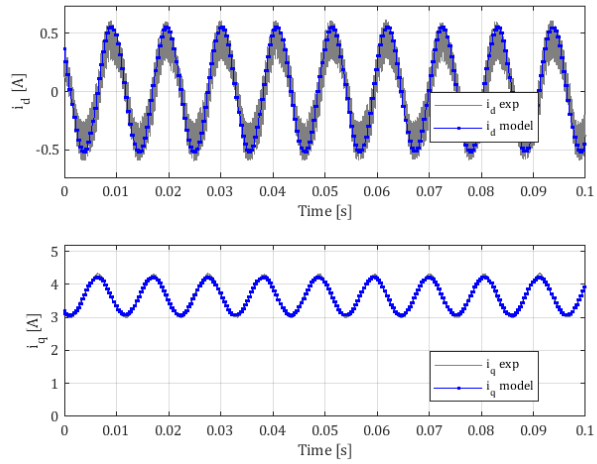

FIGURE 16. Current components i_d and i_q obtained by experimental test (gray) and by the proposed model (blue) in the case of $k_1 = 1$, $k_2 = 0.5$, $k_3 = 1$, load torque 3.4 Nm, and angular speed 1000 rpm.

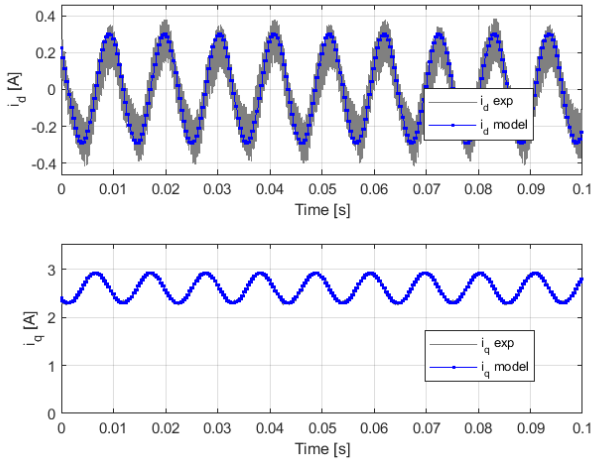

FIGURE 17. Current components i_d and i_q obtained by experimental test (gray) and by the proposed model (blue) in the case of $k_1 = 1$, $k_2 = 1.5$, $k_3 = 1$, load torque 3.4 Nm, and angular speed 1000 rpm.

Figs.18, 19, 20 and 21, for some values of the load torque, of the injected gain faults, and angular speed 1000 rpm.

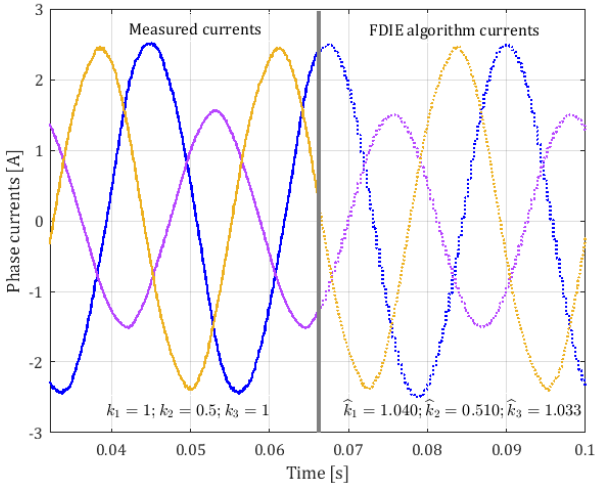

FIGURE 18. Phase currents measured by experimental test (continuous line) and evaluated by the proposed FDIE algorithm (dotted line) in the case of $k_1 = 1$, $k_2 = 0.5$, $k_3 = 1$, load torque 2.3 Nm, and angular speed 1000 rpm. The values of the current sensor gains estimated by the FDIE algorithm are: $\widehat{k}_1 = 1.040$, $\widehat{k}_2 = 0.510$, $\widehat{k}_3 = 1.033$.

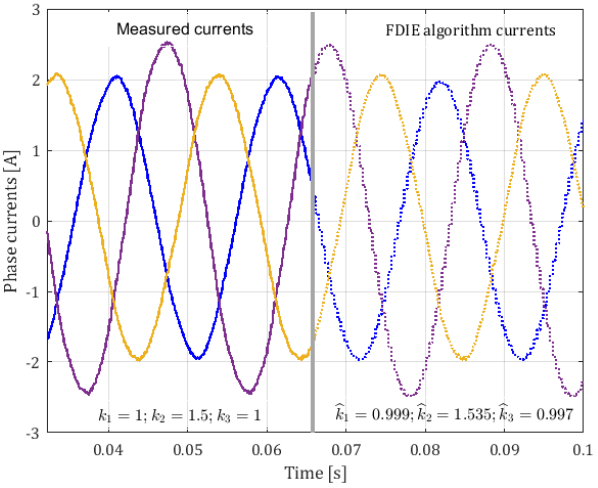

FIGURE 19. Phase currents measured by experimental test (continuous line) and evaluated by the proposed FDIE algorithm (dotted line) in the case of $k_1 = 1$, $k_2 = 1.5$, $k_3 = 1$, load torque 2.3 Nm, and angular speed 1000 rpm. The values of the current sensor gains estimated by the FDIE algorithm are: $\widehat{k}_1 = 0.999$, $\widehat{k}_2 = 1.535$, $\widehat{k}_3 = 0.997$.

The dotted lines depict the estimated currents. Besides, in these figures the estimated values of current sensors gains are reported as well. As it is possible to note, the diagnostic algorithm based on the proposed model gives very accurate results, with a maximum percentage error of about 4%. Similar results are obtained under other values of load torque, speed and faults of the sensors gains.

A. VALIDATION FOR LOW GAIN VALUES

In order to avoid mechanical damages on the test bench, the cases corresponding to zero or near zero sensors gains have not been investigated in experimental tests. In fact, these conditions determine high values of oscillation on i_q, which are directly responsible of large torque oscillations on SMPMSM

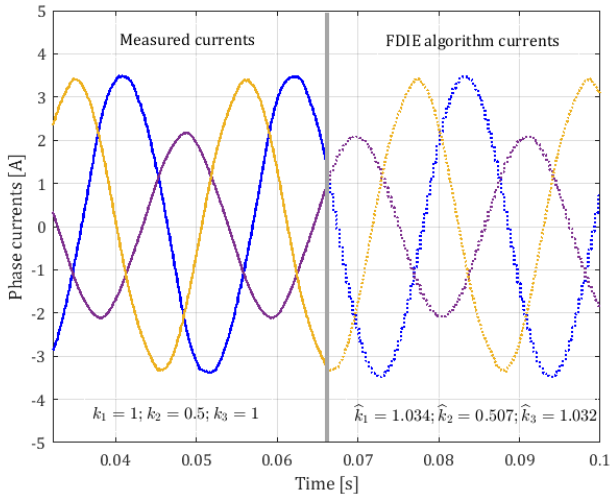

FIGURE 20. Phase currents measured by experimental test (continuous line) and evaluated by the proposed FDIE algorithm (dotted line) in the case of $k_1 = 1$, $k_2 = 0.5$, $k_3 = 1$, load torque 3.4 Nm, and angular speed 1000 rpm. The values of the current sensor gains estimated by the FDIE algorithm are: $\widehat{k}_1 = 1.034$, $\widehat{k}_2 = 0.507$, $\widehat{k}_3 = 1.032$.

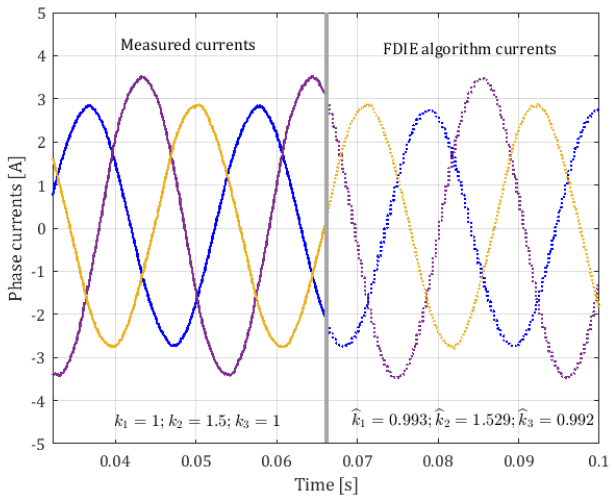

FIGURE 21. Phase currents measured by experimental test (continuous line) and evaluated by the proposed FDIE algorithm (dotted line) in the case of $k_1 = 1$, $k_2 = 1.5$, $k_3 = 1$, load torque 3.4 Nm, and angular speed 1000 rpm. The values of the current sensor gains estimated by the FDIE algorithm are: $\widehat{k}_1 = 0.993$, $\widehat{k}_2 = 1.529$, $\widehat{k}_3 = 0.992$.

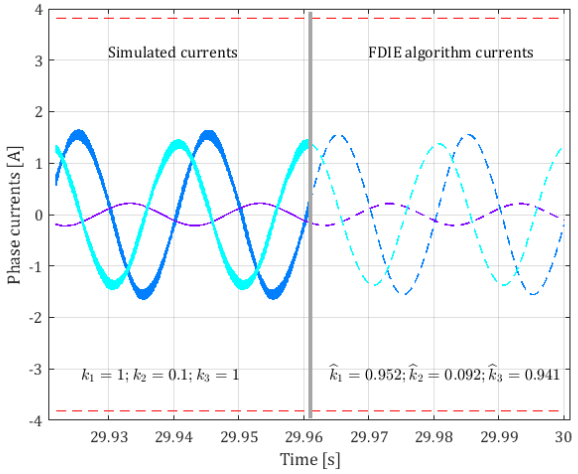

FIGURE 22. Phase currents simulated (continuous line) and evaluated by the proposed FDIE algorithm (dotted line) in the case of $k_1 = 1$, $k_2 = 0.1$, $k_3 = 1$, load torque 1.15 Nm, and angular speed 1000 rpm. The values of the current sensor gains estimated by the FDIE algorithm are: $\widehat{k}_1 = 0.952$, $\widehat{k}_2 = 0.092$, $\widehat{k}_3 = 0.941$. The dotted red lines represent the maximum peak-to-peak value of the rated current.

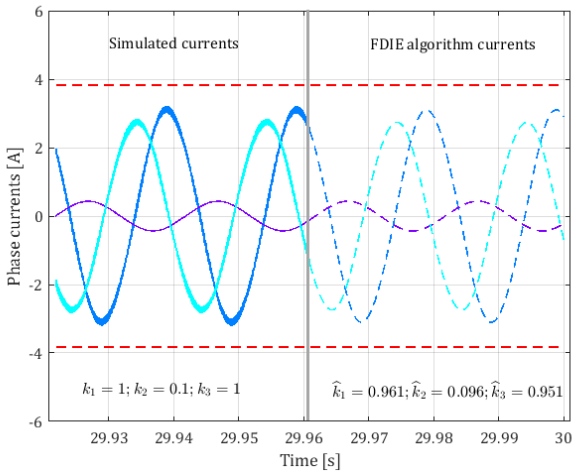

FIGURE 23. Phase currents simulated (continuous line) and evaluated by the proposed FDIE algorithm (dotted line) in the case of $k_1 = 1$, $k_2 = 0.1$, $k_3 = 1$, load torque 2.3 Nm, and angular speed 1000 rpm. The values of the current sensor gains estimated by the FDIE algorithm are: $\widehat{k}_1 = 0.961$, $\widehat{k}_2 = 0.096$, $\widehat{k}_3 = 0.951$. The dotted red lines represent the maximum peak-to-peak value of the rated current.

under test and on the Magtrol brake. However, the proposed FDIE algorithm is capable to handle faults corresponding to very low values of the gains as well. As an example, in this subsection is reported the simulation validation of the proposed FDIE algorithm considering gain values near the zero. In particular, it is analyzed the case $k_1 = 1, k_2 = 0.1, k_3 = 1$, with angular speed 1000 rpm and load torque 1.15 Nm, 2.3 Nm and 3.4 Nm. The parameters of the electrical drive and control system are the same reported in Tab.1. The results are depicted in Figs. 22, 23 and 24, where the simulated currents are compared with the currents reconstructed by the proposed FDIE algorithm. In the figures are also depicted two dotted red lines, corresponding to the maximum peak-to-peak value of SPMSM motor rated current.

From the results, it is easy to note the correct performance of the FDIE algorithm also in the case of low gain values: in fact, the estimated values of gains differ at most of 8% from the imposed ones. It is interesting to analyze the behavior at rated load condition, where the low value of the gain k_2 determines that the maximum value of currents exceeds the rated current of the motors, giving rise to an abnormal heating of the motor and triggering the drive protections.

B. PARAMETERS SENSITIVITY ANALYSIS

The analysis of sensitivity against parameters' uncertainty is a crucial point of all model-based algorithms, even if not always adequately addressed in technical literature. Of course, motor parameters R and L can be estimated by

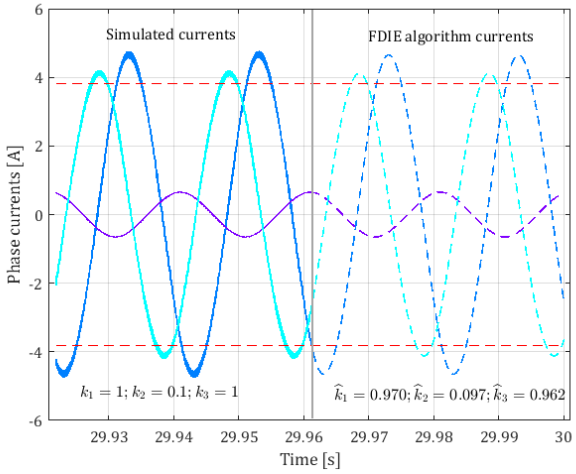

FIGURE 24. Phase currents simulated (continuous line) and evaluated by the proposed FDIE algorithm (dotted line) in the case of $k_1 = 1$, $k_2 = 0.1$, $k_3 = 1$, load torque 3.4 Nm, and angular speed 1000 rpm. The values of the current sensor gains estimated by the FDIE algorithm are: $\widehat{k}_1 = 0.970$, $\widehat{k}_2 = 0.097$, $\widehat{k}_3 = 0.962$. The dotted red lines represent the maximum peak-to-peak value of the rated current.

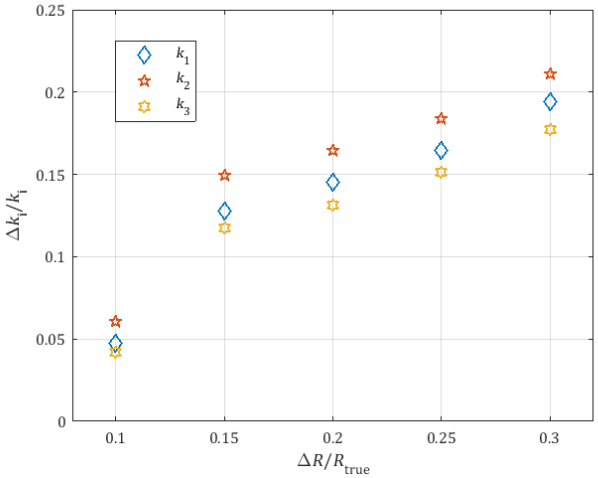

FIGURE 25. Sensitivity analysis to resistance variations: p.u. deviation Δk_i of the estimated gains $\hat{k}_i$ with respect to the true values k_i, with $i \in \{1, 2, 3\}$, as a function of the p.u. deviation ΔR of the resistance R from the true value R_{true}, in the case of $k_1 = 1$, $k_2 = 0.5$, $k_3 = 1$, load torque 3.4 Nm, angular speed 1000 rpm.

means of accurate short-circuit and open-circuit tests, but they will inevitably change with operating temperature, speed and aging of the motor. In order to assess the sensitivity of the proposed FDIE algorithm to R and L variations, many simulations have been carried out by imposing deviations ΔR, ΔL of the resistance and of the inductance from the true values R_{true} and L_{true}, respectively, and evaluating the correspondent deviations Δk_i of the estimated gains $\hat{k}_i$ from their true values k_i, with $i \in \{1, 2, 3\}$. The results obtained for the drive of tab. 1 are shown in Figs. 25 and 26, in the case of $k_1 = 1$, $k_2 = 0.5$, $k_3 = 1$, load torque 3.4 Nm, and angular speed 1000 rpm. From their inspection, it can be seen that the p.u. gain deviations are always less than the corresponding p.u. parameters deviations. Similar results are obtained for other operating conditions.

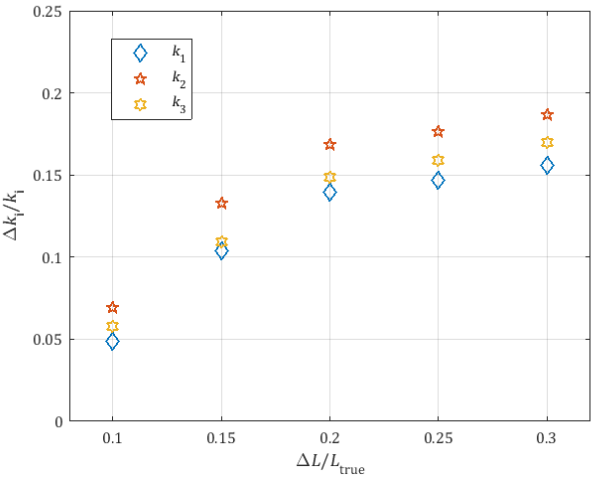

FIGURE 26. Sensitivity analysis to inductance variations: p.u. deviation Δk_i of the estimated gains $\hat{k}_i$ with respect to the true values k_i, with $i \in \{1, 2, 3\}$, as a function of the p.u. deviation ΔL of the inductance L from the true value L_{true}, in the case of $k_1 = 1$, $k_2 = 0.5$, $k_3 = 1$, load torque 3.4 Nm, angular speed 1000 rpm.

VI. CONCLUSION

In this paper a mathematical model of a SMPMSM drive with field oriented control has been developed, which is able to determine in an analytical closed form the steady-state motor currents, taking into account the effects both of the current control regulators, and of current sensors gain faults. The model has been validated by comparing its results with those obtained by means of a full Matlab® Simulink simulation of the drive. Starting from this model, an algorithm has been carried out, which allows not only to detect and isolate the current sensors affected by gain fault, but also to estimate the gain values starting from the measured values of the phase currents and motor speed, by means of a low computational cost calculation. An analysis of sensitivity to parameters variations has been carried out as well. The good agreement between numerical and experimental results confirms the validity of the proposed FDIE algorithm, which allows to detect, isolate and estimate the current sensors gain values with a very good approximation.

APPENDIX

The analytical expressions of the functions $f_{\text{d},k}$, $g_{\text{d},k}$, $f_{\text{q},k}$ and $g_{\text{q},k}$, for $k \in \{2, \ldots, n\}$, are:

$$\begin{aligned} f_{\text{d},k} = {} & \left[p\omega_{\text{r}}k(rk_{\text{pd}} - p\omega_{\text{r}}Lq) + 0.5\, qk_{\text{id}}\right] a_{\text{d},k-1} \\ & + \left[p\omega_{\text{r}}k(qk_{\text{pd}} + p\omega_{\text{r}}Lr) - 0.5\, rk_{\text{id}}\right] b_{\text{d},k-1} \\ & + \left[p\omega_{\text{r}}k(-qk_{\text{pd}} - p\omega_{\text{r}}Lr) + 0.5\, rk_{\text{id}}\right] a_{\text{q},k-1} \\ & + \left[p\omega_{\text{r}}k(rk_{\text{pd}} - p\omega_{\text{r}}Lq) + 0.5\, qk_{\text{id}}\right] b_{\text{q},k-1} \\ & + \left(-4p^2\omega_{\text{r}}^2Lk^2 + sk_{\text{id}}\right) a_{\text{d},k} + 2p\omega_{\text{r}}k\left(R + sk_{\text{pd}}\right) b_{\text{d},k} \\ & + 2p^2\omega_{\text{r}}^2Lk(s-1)\, b_{\text{q},k} \\ & + \left[p\omega_{\text{r}}k(-rk_{\text{pd}} + p\omega_{\text{r}}Lq) + 0.5\, qk_{\text{id}}\right] a_{\text{d},k+1} \\ & + \left[p\omega_{\text{r}}k(qk_{\text{pd}} + p\omega_{\text{r}}Lr) + 0.5\, rk_{\text{id}}\right] b_{\text{d},k+1} \\ & + \left[p\omega_{\text{r}}k(qk_{\text{pd}} + p\omega_{\text{r}}Lr) + 0.5\, rk_{\text{id}}\right] a_{\text{q},k+1} \\ & + \left[p\omega_{\text{r}}k(rk_{\text{pd}} - p\omega_{\text{r}}Lq) - 0.5\, qk_{\text{id}}\right] b_{\text{q},k+1} \end{aligned} \tag{39}$$

$$
\begin{aligned}
g_{\mathrm{d},k} = {} & \left[p\omega_{\mathrm{r}}k(-qk_{\mathrm{pd}} - p\omega_{\mathrm{r}}Lr) + 0.5\, rk_{\mathrm{id}}\right] a_{\mathrm{d},k-1} \\
& + \left[p\omega_{\mathrm{r}}k(rk_{\mathrm{pd}} - p\omega_{\mathrm{r}}Lq) + 0.5\, qk_{\mathrm{id}}\right] b_{\mathrm{d},k-1} \\
& + \left[p\omega_{\mathrm{r}}k(-rk_{\mathrm{pd}} + p\omega_{\mathrm{r}}Lq) - 0.5\, qk_{\mathrm{id}}\right] a_{\mathrm{q},k-1} \\
& + \left[p\omega_{\mathrm{r}}k(-qk_{\mathrm{pd}} - p\omega_{\mathrm{r}}Lr) + 0.5\, rk_{\mathrm{id}}\right] b_{\mathrm{q},k-1} \\
& - 2p\omega_{\mathrm{r}}k\left(R + sk_{\mathrm{pd}}\right)a_{\mathrm{d},k} + \left(-4p^2\omega_{\mathrm{r}}^2Lk^2 + sk_{\mathrm{id}}\right)b_{\mathrm{d},k} \\
& + 2p^2\omega_{\mathrm{r}}^2Lk(s-1)\, a_{\mathrm{q},k} \qquad (40) \\
& + \left[p\omega_{\mathrm{r}}k(-qk_{\mathrm{pd}} - p\omega_{\mathrm{r}}Lr) - 0.5\, rk_{\mathrm{id}}\right] a_{\mathrm{d},k+1} \\
& + \left[p\omega_{\mathrm{r}}k(-rk_{\mathrm{pd}} + p\omega_{\mathrm{r}}Lq) + 0.5\, qk_{\mathrm{id}}\right] b_{\mathrm{d},k+1} \\
& + \left[p\omega_{\mathrm{r}}k(-rk_{\mathrm{pd}} + p\omega_{\mathrm{r}}Lq) + 0.5\, qk_{\mathrm{id}}\right] a_{\mathrm{q},k+1} \\
& + \left[p\omega_{\mathrm{r}}k(qk_{\mathrm{pd}} + p\omega_{\mathrm{r}}Lr) + 0.5\, rk_{\mathrm{id}}\right] b_{\mathrm{q},k+1} \\
f_{\mathrm{q},k} = {} & \left[p\omega_{\mathrm{r}}k(-qk_{\mathrm{pq}} - p\omega_{\mathrm{r}}Lr) + 0.5\, rk_{\mathrm{iq}}\right] a_{\mathrm{d},k-1} \\
& + \left[p\omega_{\mathrm{r}}k(rk_{\mathrm{pq}} - p\omega_{\mathrm{r}}Lq) + 0.5\, qk_{\mathrm{iq}}\right] b_{\mathrm{d},k-1} \\
& + \left[p\omega_{\mathrm{r}}k(-rk_{\mathrm{pq}} + p\omega_{\mathrm{r}}Lq) - 0.5\, qk_{\mathrm{iq}}\right] a_{\mathrm{q},k-1} \\
& + \left[p\omega_{\mathrm{r}}k(-qk_{\mathrm{pq}} - p\omega_{\mathrm{r}}Lr) + 0.5\, rk_{\mathrm{iq}}\right] b_{\mathrm{q},k-1} \\
& - 2p^2\omega_{\mathrm{r}}^2Lk(s-1)\, b_{\mathrm{d},k} \qquad (41) \\
& + \left(-4p^2\omega_{\mathrm{r}}^2Lk^2 + sk_{\mathrm{iq}}\right)a_{\mathrm{q},k} + 2p\omega_{\mathrm{r}}k\left(R + sk_{\mathrm{pq}}\right)b_{\mathrm{q},k} \\
& + \left[p\omega_{\mathrm{r}}k(qk_{\mathrm{pq}} + p\omega_{\mathrm{r}}Lr) + 0.5\, rk_{\mathrm{iq}}\right] a_{\mathrm{d},k+1} \\
& + \left[p\omega_{\mathrm{r}}k(rk_{\mathrm{pq}} - p\omega_{\mathrm{r}}Lq) - 0.5\, qk_{\mathrm{iq}}\right] b_{\mathrm{d},k+1} \\
& + \left[p\omega_{\mathrm{r}}k(rk_{\mathrm{pq}} - p\omega_{\mathrm{r}}Lq) - 0.5\, qk_{\mathrm{iq}}\right] a_{\mathrm{q},k+1} \\
& + \left[p\omega_{\mathrm{r}}k(-qk_{\mathrm{pq}} - p\omega_{\mathrm{r}}Lr) - 0.5\, rk_{\mathrm{iq}}\right] b_{\mathrm{q},k+1} \\
g_{\mathrm{q},k} = {} & \left[p\omega_{\mathrm{r}}k(-rk_{\mathrm{pq}} + p\omega_{\mathrm{r}}Lq) - 0.5\, qk_{\mathrm{iq}}\right] a_{\mathrm{d},k-1} \\
& + \left[p\omega_{\mathrm{r}}k(-qk_{\mathrm{pq}} - p\omega_{\mathrm{r}}Lr) + 0.5\, rk_{\mathrm{iq}}\right] b_{\mathrm{d},k-1} \\
& + \left[p\omega_{\mathrm{r}}k(qk_{\mathrm{pq}} + p\omega_{\mathrm{r}}Lr) - 0.5\, rk_{\mathrm{iq}}\right] a_{\mathrm{q},k-1} \\
& + \left[p\omega_{\mathrm{r}}k(-rk_{\mathrm{pq}} + p\omega_{\mathrm{r}}Lq) - 0.5\, qk_{\mathrm{iq}}\right] b_{\mathrm{q},k-1} \\
& + 2p^2\omega_{\mathrm{r}}^2Lk(s-1)\, a_{\mathrm{d},k} \\
& - 2p\omega_{\mathrm{r}}k\left(R + sk_{\mathrm{pq}}\right)a_{\mathrm{q},k} + \left(-4p^2\omega_{\mathrm{r}}^2Lk^2 + sk_{\mathrm{iq}}\right)b_{\mathrm{q},k} \\
& + \left[p\omega_{\mathrm{r}}k(-rk_{\mathrm{pq}} + p\omega_{\mathrm{r}}Lq) + 0.5\, qk_{\mathrm{iq}}\right] a_{\mathrm{d},k+1} \\
& + \left[p\omega_{\mathrm{r}}k(qk_{\mathrm{pq}} + p\omega_{\mathrm{r}}Lr) + 0.5\, rk_{\mathrm{iq}}\right] b_{\mathrm{d},k+1} \\
& + \left[p\omega_{\mathrm{r}}k(qk_{\mathrm{pq}} + p\omega_{\mathrm{r}}Lr) + 0.5\, rk_{\mathrm{iq}}\right] a_{\mathrm{q},k+1} \\
& + \left[p\omega_{\mathrm{r}}k(rk_{\mathrm{pq}} - p\omega_{\mathrm{r}}Lq) - 0.5\, qk_{\mathrm{iq}}\right] b_{\mathrm{q},k+1} \qquad (42)
\end{aligned}
$$

Equations (39), (40), (41), (42) can be used also to determine $f_{\mathrm{d},1}$, $g_{\mathrm{d},1}$, $f_{\mathrm{q},1}$, $g_{\mathrm{q},1}$, $f_{\mathrm{d},n+1}$, $g_{\mathrm{d},n+1}$, $f_{\mathrm{q},n+1}$ and $g_{\mathrm{q},n+1}$. In particular, $f_{\mathrm{d},1}$, $g_{\mathrm{d},1}$, $f_{\mathrm{q},1}$, $g_{\mathrm{q},1}$ are obtained from (39), (40), (41), (42), respectively, by setting equal to zero the coefficients having subscript 0 and adding the following terms:

$$
\begin{aligned}
\text{to (39)}: \quad & \left[2p\omega_{\mathrm{r}}(rk_{\mathrm{pd}} - p\omega_{\mathrm{r}}Lq) + qk_{\mathrm{id}}\right] c_{\mathrm{d}} \\
& + \left[-2p\omega_{\mathrm{r}}(qk_{\mathrm{pd}} + p\omega_{\mathrm{r}}Lr) + rk_{\mathrm{id}}\right] c_{\mathrm{q}} \qquad (43) \\
\text{to (40)}: \quad & \left[-2p\omega_{\mathrm{r}}(qk_{\mathrm{pd}} + p\omega_{\mathrm{r}}Lr) + rk_{\mathrm{id}}\right] c_{\mathrm{d}} \\
& + \left[-2p\omega_{\mathrm{r}}(rk_{\mathrm{pd}} - p\omega_{\mathrm{r}}Lq) - qk_{\mathrm{id}}\right] c_{\mathrm{q}} \qquad (44) \\
\text{to (41)}: \quad & \left[-2p\omega_{\mathrm{r}}(qk_{\mathrm{pq}} + p\omega_{\mathrm{r}}Lr) + rk_{\mathrm{iq}}\right] c_{\mathrm{d}} \\
& + \left[-2p\omega_{\mathrm{r}}(qk_{\mathrm{pq}} - p\omega_{\mathrm{r}}Lr) - rk_{\mathrm{iq}}\right] c_{\mathrm{q}} \qquad (45) \\
\text{to (42)}: \quad & \left[-2p\omega_{\mathrm{r}}(rk_{\mathrm{pq}} - p\omega_{\mathrm{r}}Lq) - qk_{\mathrm{iq}}\right] c_{\mathrm{d}} \\
& + \left[2p\omega_{\mathrm{r}}(qk_{\mathrm{pq}} + p\omega_{\mathrm{r}}Lr) - rk_{\mathrm{iq}}\right] c_{\mathrm{q}} \qquad (46)
\end{aligned}
$$

while $f_{\mathrm{d},n+1}$, $g_{\mathrm{d},n+1}$, $f_{\mathrm{q},n+1}$, $g_{\mathrm{q},n+1}$ are simply obtained by setting equal to zero the coefficients having subscript $n+2$.

Eventually, the analytical expressions of the functions $f_{\mathrm{d},0}$ and $f_{\mathrm{q},0}$ are:

$$
\begin{aligned}
f_{\mathrm{d},0} &= 0.5\, k_{\mathrm{id}}\left(qa_{\mathrm{d},1} + rb_{\mathrm{d},1} + ra_{\mathrm{q},1} - qb_{\mathrm{q},1} + sc_{\mathrm{d}}\right) \qquad (47) \\
f_{\mathrm{q},0} &= 0.5\, k_{\mathrm{iq}}\left(ra_{\mathrm{d},1} - qb_{\mathrm{d},1} - qa_{\mathrm{q},1} - rb_{\mathrm{q},1} + sc_{\mathrm{q}}\right) \qquad (48)
\end{aligned}
$$

REFERENCES

[1] Z. Yang, F. Shang, I. P. Brown, and M. Krishnamurthy, "Comparative study of interior permanent magnet, induction, and switched reluctance motor drives for EV and HEV applications," *IEEE Trans. Transport. Electrific.*, vol. 1, no. 3, pp. 245–254, Oct. 2015.

[2] D. G. Dorrell, M. Hsieh, M. Popescu, L. Evans, D. A. Staton, and V. Grout, "A review of the design issues and techniques for radial-flux brushless surface and internal rare-earth permanent-magnet motors," *IEEE Trans. Ind. Electron.*, vol. 58, no. 9, pp. 3741–3757, Sep. 2011.

[3] J. de Santiago, H. Bernhoff, B. Ekergård, S. Eriksson, S. Ferhatovic, R. Waters, and M. Leijon, "Electrical motor drivelines in commercial all-electric vehicles: A review," *IEEE Trans. Veh. Technol.*, vol. 61, no. 2, pp. 475–484, Feb. 2012.

[4] Y. Duan and D. M. Ionel, "A review of recent developments in electrical machine design optimization methods with a permanent-magnet synchronous motor benchmark study," *IEEE Trans. Ind. Appl.*, vol. 49, no. 3, pp. 1268–1275, Jun. 2013.

[5] S. Khojet El Khil, I. Jlassi, A. J. Marques Cardoso, J. O. Estima, and N. Mrabet-Bellaaj, "Diagnosis of open-switch and current sensor faults in PMSM drives through stator current analysis," *IEEE Trans. Ind. Appl.*, vol. 55, no. 6, pp. 5925–5937, Nov. 2019.

[6] X. Ding, Y. Zhang, and Z. Ye, "Current sensors offset fault online estimation in permanent magnet synchronous generator (PMSG) drives for offshore wind turbines," *IEEE Access*, vol. 9, pp. 135996–136003, 2021.

[7] L. Guo and J. Ye, "Cyber-physical security of electric vehicles with four motor drives," *IEEE Trans. Power Electron.*, vol. 36, no. 4, pp. 4463–4477, Apr. 2021.

[8] B. Lu and V. C. Gungor, "Online and remote motor energy monitoring and fault diagnostics using wireless sensor networks," *IEEE Trans. Ind. Electron.*, vol. 56, no. 11, pp. 4651–4659, Nov. 2009.

[9] S. Choi, M. S. Haque, M. T. B. Tarek, V. Mulpuri, Y. Duan, S. Das, V. Garg, D. M. Ionel, M. A. Masrur, B. Mirafzal, and H. A. Toliyat, "Fault diagnosis techniques for permanent magnet AC machine and drives—A review of current state of the art," *IEEE Trans. Transport. Electrific.*, vol. 4, no. 2, pp. 444–463, Jun. 2018.

[10] I.-H. Kao, W.-J. Wang, Y.-H. Lai, and J.-W. Perng, "Analysis of permanent magnet synchronous motor fault diagnosis based on learning," *IEEE Trans. Instrum. Meas.*, vol. 68, no. 2, pp. 310–324, Feb. 2019.

[11] B. Gou, Y. Xu, Y. Xia, G. Wilson, and S. Liu, "An intelligent time-adaptive data-driven method for sensor fault diagnosis in induction motor drive system," *IEEE Trans. Ind. Electron.*, vol. 66, no. 12, pp. 9817–9827, Dec. 2019.

[12] B. Cai, Y. Zhao, H. Liu, and M. Xie, "A data-driven fault diagnosis methodology in three-phase inverters for PMSM drive systems," *IEEE Trans. Power Electron.*, vol. 32, no. 7, pp. 5590–5600, Jul. 2017.

[13] Y. L. Murphey, M. A. Masrur, Z. Chen, and B. Zhang, "Model-based fault diagnosis in electric drives using machine learning," *IEEE/ASME Trans. Mechatronics*, vol. 11, no. 3, pp. 290–303, Jun. 2006.

[14] K. Choi, Y. Kim, S.-K. Kim, and K.-S. Kim, "Current and position sensor fault diagnosis algorithm for PMSM drives based on robust state observer," *IEEE Trans. Ind. Electron.*, vol. 68, no. 6, pp. 5227–5236, Jun. 2021.

[15] W. Wang, W. Tian, Z. Wang, W. Hua, and M. Cheng, "A fault diagnosis method for current sensors of primary permanent-magnet linear motor drives," *IEEE Trans. Power Electron.*, vol. 36, no. 2, pp. 2334–2345, Feb. 2021.

[16] C. Wu, C. Guo, Z. Xie, F. Ni, and H. Liu, "A signal-based fault detection and tolerance control method of current sensor for PMSM drive," *IEEE Trans. Ind. Electron.*, vol. 65, no. 12, pp. 9646–9657, Dec. 2018.

[17] T. Shen, Y. Chen, C. Thulfaut, and H.-C. Reuss, "A data based diagnostic method for current sensor fault in permanent magnet synchronous motors (PMSM)," in *Proc. 45th Annu. Conf. IEEE Ind. Electron. Soc. (IECON)*, vol. 1, Oct. 2019, pp. 5979–5985.

[18] M. C. Harke and R. D. Lorenz, "The spatial effect and compensation of current sensor differential gains for three-phase three-wire systems," *IEEE Trans. Ind. Appl.*, vol. 44, no. 4, pp. 1181–1189, Jul. 2008.

[19] J.-I. Itoh, Y. Ikarashi, K. Nishizawa, and H. Tamura, "Torque ripple reduction method of permanent magnet synchronous motor by current sensor gain unbalance correction," in *Proc. IEEE 2nd Int. Future Energy Electron. Conf. (IFEEC)*, Nov. 2015, pp. 1–5.
[20] M. Kim, S.-K. Sul, and J. Lee, "Compensation of current measurement error for current-controlled PMSM drives," *IEEE Trans. Ind. Appl.*, vol. 50, no. 5, pp. 3365–3373, Sep. 2014.
[21] Z. Gao, C. Cecati, and S. X. Ding, "A survey of fault diagnosis and fault-tolerant techniques—Part I: Fault diagnosis with model-based and signal-based approaches," *IEEE Trans. Ind. Electron.*, vol. 62, no. 6, pp. 3757–3767, Mar. 2015.
[22] B. K. Bose, *Power Electronics and AC Drives*. Bergen, NJ, USA: Englewood Cliffs, 1986.
[23] W. Leonhard, *Control of Electrical Drives*. Berlin, Germany: Springer, 2001.
[24] W. E. Boyce, R. C. DiPrima, and D. B. Meade, *Elementary Differential Equations and Boundary Value Problems*. Hoboken, NJ, USA: Wiley, 2021.
[25] K. F. Riley, M. P. Hobson, and S. J. Bence, *Mathematical Methods for Physics and Engineering*. Cambridge, U.K.: Cambridge Univ. Press, 1999.

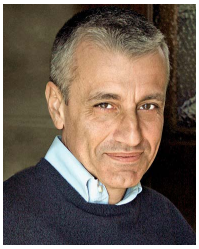

CIRO ATTAIANESE (Senior Member, IEEE) received the M.Sc. and Ph.D. degrees in electrical engineering from the University of Naples "Federico II," Italy, in 1983 and 1989, respectively. In 1984, he joined Procter & Gamble Company as an Industrial Engineer. In 1985, he had a traineeship at Ansaldo Trasporti, Naples, working on the design of electric drives for railway traction. From January 1990 to October 1992, he was a Researcher in electrical machines, power electronics and electric drives with the Faculty of Engineering, University of Naples "Federico II." In November 1992, he joined the University of Cassino and Southern Lazio as an Associate Professor in electrical machines, power electronics, and electric drives, where he became a Full Professor, in November 1999. At the University of Cassino and Southern Lazio, he was the Head of the Laboratory of Industrial Automation and the Laboratory of Electromagnetic Compatibility. From 1999 to 2008, he was the Chair of the Ph.D. School in Power Electronics, Electrical Machine and Electrical Drives. From November 2009 to October 2015, he was the Rector of the University of Cassino and Southern Lazio, and from May 2013 to October 2015, he was the President of CRUL, the Association of the Universities of Lazio. In December 2019, he joined the University of Naples "Federico II." He is currently the Founder of three startups operating in the field of power electronics and e-mobility. He is also the President of the inter-university consortium ELMO—Electrification of Mobility that brings together 15 Italian universities operating in the e-mobility. His current research interests include electrical machines and power converters modeling, electrical drives and applications of microprocessors to their control, renewable energy, and electrification of mobility.

MATILDE D'ARPINO (Member, IEEE) received the B.S. and M.S. degrees in electrical engineering and the Ph.D. degree in systems, technologies, and devices for movement and health from the University of Cassino, Italy, in 2008, 2010, and 2014, respectively. Since 2016, she has been a Researcher at the Center for Automotive Research, The Ohio State University, Columbus, OH, USA. Her research interests include design and control of electric vehicle for automotive and aerospace, power converters and energy management controls for multi-source power systems (e.g., microgrids, hybrid vehicles, and hybrid aircraft), testing, modeling, design, control, and diagnostic of energy storage systems.

MAURO DI MONACO (Member, IEEE) was born in Cassino, Italy, in October 1981. He received the B.Sc. degree in electrical engineering and the Ph.D. degree from the University of Cassino, Italy, in 2006 and 2010, respectively. Since 2010, he has been a Researcher with the Laboratory of Industrial Automation, University of Cassino and Southern Lazio. His research interests include the study and the implementation of new optimization algorithms and modulation techniques for multi-level and multi-source power converters in the fields of renewable energy and e-mobility, new powertrain architectures, and control techniques for electric vehicles.

LUIGI PIO DI NOIA (Senior Member, IEEE) received the M.S. and Ph.D. degrees in electrical engineering from the University of Naples "Federico II," Napoli, Italy, in 2011 and 2015, respectively. Since 2018, he has been a Research Fellow of Electrical Machines, Power Electronics and Electric Drives. His research interests include the design and control of electrical machines and drives for electrification of traction and propulsion, fault diagnosis, and prognostic.